



Pattern and variation of electron ionisation gradient as related to the plasma distribution mechanisms during the total solar eclipse of March 20, 2015

B. J. Adekoya ^{a,*}, B. O. Adebesein ^{b,c}, V. U. Chukwuma ^a, S. J. Adebisi ^d, S. O. Ikubanni ^d,
H. T. Oladunjoye ^a, E. O. Adekoya^a

^aDepartment of Physics, Olabisi Onabanjo University, P.M.B. 2002, Ago Iwoye, Nigeria

^bDepartment of Physical Sciences, Hillside University of Science and Technology, Okemesi Ekiti State Nigeria

^cDepartment of Aerospace Engineering, Hillside University of Science and Technology, Okemesi Ekiti State Nigeria

^dSpace Weather Group, Department of Physical Sciences, Landmark University, P.M.B. 1001, Omu-Aran, Kwara State, Nigeria

Abstract

The pattern and electron ionisation gradient associated with the obstruction of solar ionising radiation (SIR) provided a good opportunity to study the plasma movements and neutral compositions during the solar eclipse at mid-latitude. The electron ionisation gradient (dN/dh) related to the plasma distributions at the mid-latitudes during the total solar eclipse of 20 March 2015 was investigated. The ionogram inversion profile data for each station along the solar eclipse path were obtained from the Global Ionospheric Radio Observatory (GIRO) database. The solar eclipse's obscuration percentage at these locations ranges from 69% to 94%. The variations in the dN/dh and its corresponding height h_{dN} during the eclipse window are related to the solar eclipse's turnoff and onset effect on SIR. The ionisation gradient valley caused by the solar eclipse was associated with the vertical transport and diffusion processes. The dN/dh varies correspondingly with NmF2, responding to changes in photoionisation, and the peak responses occurred 11 – 20 mins after the eclipse's totality. The height (h_{dN}) at which the maximum ionisation gradient was obtained followed a similar pattern to hmF2, but the peak response of h_{dN} is lower across all stations. In contrast to the hmF2, the time lag between the ionisation gradient's minimum peak and the eclipse's maximum magnitude ranges from 25 to 40 mins. The neutral composition changes and plasma movements during the solar eclipse can be explained by dN/dh .

DOI:10.46481/jnsps.2025.2209

Keywords: Ionisation gradient, photoionisation, total solar eclipse, electron density profile, NmF2

Article History :

Received: 22 June 2024

Received in revised form: 05 October 2024

Accepted for publication: 07 December 2024

Available online: 08 February 2025

© 2025 The Author(s). Published by the Nigerian Society of Physical Sciences under the terms of the Creative Commons Attribution 4.0 International license. Further distribution of this work must maintain attribution to the author(s) and the published article's title, journal citation, and DOI.


Communicated by: C. A. Onate

1. Introduction

Solar eclipses are an intriguing phenomenon of astronomical events that are related to variations in ionospheric electron density and irregularities caused by changes in SIR. It offers the opportunity to study the ionospheric F2 formation and transport processes at the mid-latitude region. During a solar eclipse, the

*Corresponding author Tel. No: +234-815-512-3736

Email address: adekoya.bolarinwa@oouagoiwoye.edu.ng (B. J.

Adekoya )

amount of solar ionizing radiation (SIR) reaching the Earth's ionosphere is reduced due to the Moon's shadow [1–3]. Hence, the changes in the structure and pattern of the electron density profile at the ionospheric altitudes. Since the radio wave signal travels through different parts of the ionospheric electron density profile depending on the level of the accumulated effect due to the removal of the SIR. Therefore, understanding the pattern and variation of the electron ionisation gradient during a solar eclipse is of great importance. The ionospheric disturbance, especially at F2-region is not limited to radio propagation alone but also affects the communication system as well as the navigation system of satellites. Chukwuma and Adekoya [4] claimed that the effects of solar eclipses on the ionosphere reflect multiple intricate processes related to the electrodynamics of the ionosphere and ionisation profile gradients, such as photochemistry, transport and diffusion mechanisms, and potential perturbations to the neutral atmosphere brought on by its cooling processes.

In the mid-latitude, solar radiation, electron density changes, geomagnetic effects, the vertical transport process, neutral composition changes, and atmospheric waves and tides are among the primary factors that can affect the diffusion mechanisms of ionospheric F2 plasma during solar eclipse [1, 2, 4–19]. Solar radiation: during a solar eclipse, the Earth experiences a sudden reduction in solar radiation, including ultraviolet (UV) and extreme ultraviolet (EUV) radiation [7, 8]. The short-time removal of solar radiation during the daytime can adversely affect ionisation and photochemical processes in the F2 region of the ionosphere [1, 2, 6, 20]. Electron density in the ionosphere varies with the daily solar ionising radiation, which decreases with reduced solar radiation in the F2 region. The reduction in ionisation rates and recombination processes contributes to decreased electron density. This, in turn, affects the diffusion mechanisms of the F2 plasma [9, 12, 21]. Temperature Changes: Muller-Wodarg *et al.* [6] and Rishbeth [20] established that solar eclipses could cause temperature and wind changes in the upper atmosphere, altering the composition and density of neutral particles. The variations in neutral composition can affect plasma diffusion by modifying ion-neutral interaction rates and associated collision frequencies [6, 20]. Also, Adekoya *et al.* [2] have shown that the reduction in temperature during a solar eclipse event influences the scale height of ionospheric layers, thereby, altering the vertical distribution of ions and electrons. Plasma drift/Electric field: the reduced solar radiation and resulting changes in electron density can induce plasma drifts in the F2 region. Plasma drifts refer to the movement of ionospheric plasma under the influence of electric fields [22–25]. During a solar eclipse, the reduction in ionospheric conductivity can lead to changes in the electric fields, plasma density gradient and gravity, affecting plasma drifts and diffusion [2, 4, 16, 25]. Meza *et al.* [26] have noted that any process that influences ionospheric conductivity affects the electric current. Geomagnetic field: Research has confirmed that eclipse-induced ionosphere disturbances could interact with the Earth's geomagnetic field, resulting in intricate ionospheric responses. Geomagnetic field can modify plasma convection patterns and magnetic field configurations, influencing the diffusion mecha-

nisms [27].

Atmospheric waves: The absorption of solar energy, its redistribution, and the gravitational forces exerted by the Moon's shadow can all induce oscillatory motion in the atmosphere. Through their effects on neutral winds and electric fields, these waves can propagate upward into the ionosphere and influence plasma dynamics, including diffusion mechanisms [27]. The sudden reduction in solar heating can cause fluctuation in the temperature and pressure of the atmosphere. These variations can propagate to the ionosphere and influence ionospheric density and diffusion, which may lead to diurnal waves [28–30]. A solar eclipse can temporarily alter the distribution of gravitational forces in the Earth-Moon-Sun system, which may lead to variations in semidiurnal atmospheric tides.

It is significant to note that the local diffusion processes and their impacts during a solar eclipse might vary depending on some variables, such as the length of the eclipse, the geographic location of the mid-latitude region, and the local atmospheric and ionospheric conditions. Detailed observations and modelling studies have been typically conducted to understand the specific diffusion mechanisms during solar eclipses in different regions. However, this paper only relates the ionisation gradient to the basic diffusion mechanisms associated with the sudden removal of ionising solar radiation during the daytime, as a possible way of explaining the induced solar eclipse effect on the ionosphere at mid-latitude.

In the last few decades, progress has been made in studying the effect of the solar eclipse on the ionosphere electron density structure and dynamics. Different methods and techniques have been employed in explaining the plasma distribution during solar eclipses. At mid-latitudes, diffusion mechanisms have been established to explain the sudden removal of the solar eclipse [1, 2, 4, 6, 12, 15, 18, 19, 21, 25, 31–34]. However, the ionisation gradient can be explained in terms of plasma dynamics in the mid-latitude region. Its structure maps out the electron density profile at different altitudes of the ionosphere through which the radio wave signal travels. During a solar eclipse, changes in the ionosphere ionization gradients can affect the radio wave propagation across the ionosphere. This may subsequently lead to variations in communication and navigation systems relying on ionospheric propagation. Adebessin *et al.* [35] have established an inverse relationship between the pattern of electron ionisation gradient, dN/dh and plasma electrodynamics/vertical plasma drift at an equatorial latitude, it was therefore used in quantifying the plasma irregularities at the ionospheric F2-layer. Moreover, Adebessin *et al.* [35] have suggested the use of dN/dh characteristics as proxies for inferring the characteristic of the vertical plasma velocity. Therefore, the pattern and variation of dN/dh may further the understanding of the fundamental dynamics and plasma distribution in the mid-latitude region during a solar eclipse. The knowledge can improve the understanding of the characteristics of the plasma dynamic structure of the ionosphere, the ionosphere formation and more importantly the anomalies brought during the short time removal of the SIR.

2. Data and method

As seen in Figure 1, the total solar eclipse was visible in Iceland, Europe, North Africa, and North Asia. It travelled via the North Atlantic, Faeroe Island, and Svalbard in the northern hemisphere (<https://eclipse.gsfc.nasa.gov/SEdecade/SEdecade2011.html>). Table 1 highlights the local circumstances of the solar eclipse, as well as the times of the first, middle, and last contact of the investigated ionospheric stations. More information about the total solar eclipse event, its partiality, the conditions underlying its evolution, and the obscuration magnitude obtained from http://xjubier.free.fr/en/index_en.html. The selection of stations was influenced by the eclipse's course. Using the digital ionogram data from (<http://giro.uml.edu/DIDBase>) [36] and manually validated, the Global Ionospheric Radio Observatory (GIRO) networks provided the ionospheric data for the study's chosen mid-latitude stations. Access to autoscaled values of ionospheric parameters produced by the UMLCAR-SAO Explorer's built-in automatic real-time ionogram scaler with true height (ARTIST) algorithm is made possible via the GIRO [36–38]. ARTIST software scales the ionogram and calculates the vertical electron density profile in real-time [37, 39].

The profile peak of the electron density of the F2-region values during the eclipse (NmF2e) and the control day (NmF2c) were calculated from their respective critical frequency (foF2) using the following expression $NmF2 = ((foF2)^2 / 80.5) \text{ e/m}^{-3}$ [40, 41]. The foF2 is measured in Hertz. The average of the two days preceding and following the eclipse day, that is, March 18, 19, 22, and 23, is the value of the control day. These days were carefully chosen such that their solar and geomagnetic activity classifications are the same as those of the solar eclipse day. This will allow the observation of the real changes caused by the solar eclipse in the ionosphere. The ionospheric parameters for these studied periods are tagged with the suffix “e” for the eclipse day and “c” for the control day. The daily average of the interplanetary index, Ap, is 22 nT, the Kp index is 3.7, and the solar flux index is $F10.7 = 111.8 \text{ sfu}$ (1 solar flux unit (sfu) = $10^{-22} \text{ Wm}^{-2}\text{Hz}^{-1}$). Similarly, the control days' solar and geomagnetic activities fall within the range of classification for perturbed geomagnetic conditions, using Kp, Ap and F10.7 [4, 25]. The respective geomagnetic activity classification for the reference days (i.e. March 18, 19, 22 and 23) are as follows; Kp index – 5, 3.7, 3.0 and 3.3; Ap index – 47, 26, 24, and 19 nT; F10.7 index – 113.7, 108.3, 112.7 and 121.5 sfu, which indicates the geomagnetic active periods [31]. The National Space Science Data Centre (NSSDC) provided the daily average of the Kp, Ap, and solar flux indices through its OMNI database, which may be accessed at <https://omniweb.gsfc.nasa.gov>.

The hmF2 is the peak height corresponding to the maximum electron density of the F2 layer (NmF2). The ionisation gradient profile, dN/dh is the changes in the electron density (N) with respect to altitude (h), (i.e., dN/dh) [35, 42, 43]. The ionisation density gradient refers to the change in the electron concentration or density with respect to distance in a particular region of the atmosphere. It represents the variation in the number of electrons per unit volume as they move through the atmosphere.

For the observation of the F2-region electron ionisation gradient (dN/dh) profile, the heights above 180 km altitude to the F2 upper bound were considered. The ionisation density gradient is often used to study phenomena like the ionosphere, where ionisation of atmospheric gases occurs due to solar radiation [35, 42]. By measuring the ion density at different altitudes and calculating the ionisation density gradient, one can understand the structure and behaviour of the ionosphere, including its layers and variations. The reason was that during a solar eclipse, the F – region assumes a partial nighttime mode where the F1 layer tends to become less distinct or even disappear temporarily during the eclipse. The F2-layer plasma is composed mainly of O^+ ; during the eclipse window, it moves downward towards lower altitudes where the neutral density is higher. This results in a lowering of the F2 layer altitude during the eclipse. The F1 layer may merge with the F2 layer, and the F2 layer altitude may decrease during a solar eclipse due to reduced ionisation, increased recombination, and downward plasma motion driven by ambipolar diffusion. These effects are temporary and typically return to their normal state after the eclipse period. These parameters will provide information on the ionosphere formation, ionisation gradient, thermospheric composition, neutral winds and plasma movement in response to the removal of SIR during the daytime.

3. Results and discussion

3.1. Ionospheric parameters response to the solar eclipse

This section presents the variation of ionospheric parameters observed over mid-latitude stations during the total solar eclipse of 20 March 2015. All the stations are within a narrow longitude range, and the eclipse over the stations is observed concurrently. Figure 2 shows the time variation of the electron density, NmF2 (first column) and its associated peak height, hmF2 (second column) as the moon passed over the stations, obscuring the ionizing radiation. The variation in NmF2e and hmF2e during the solar eclipse was compared to that of the control day (NmF2c and hmF2c) to observe the solar eclipse-related effect on the ionosphere. The continuous line represents the variations during the eclipse day, while the control day is denoted by the dashed line. The vertical lines denote the progression of the solar eclipse circumstances; the lines represent the start time of the eclipse (S), the maximum magnitude of the eclipse (M) and the last contact of the eclipse (E), respectively. During the solar eclipse window, there are two distinct phases of eclipse progression: the first phase is between the start time of the eclipse and the maximum magnitude of the eclipse, and the second is between the eclipse's peak magnitude and its last phase.

Figure 2a depicts the NmF2 and hmF2 excursion over El Arenosilo in response to the solar eclipse compared to the control day variation. The observation shows that ionisation decreases from the eclipse's first contact through the maximum contact of the eclipse to the end time as against the continuous increase in NmF2c. The NmF2e decreased from $0.46 \times 10^{12} \text{ e/m}^3$ at the eclipse start time and reached a minimum of $0.31 \times$

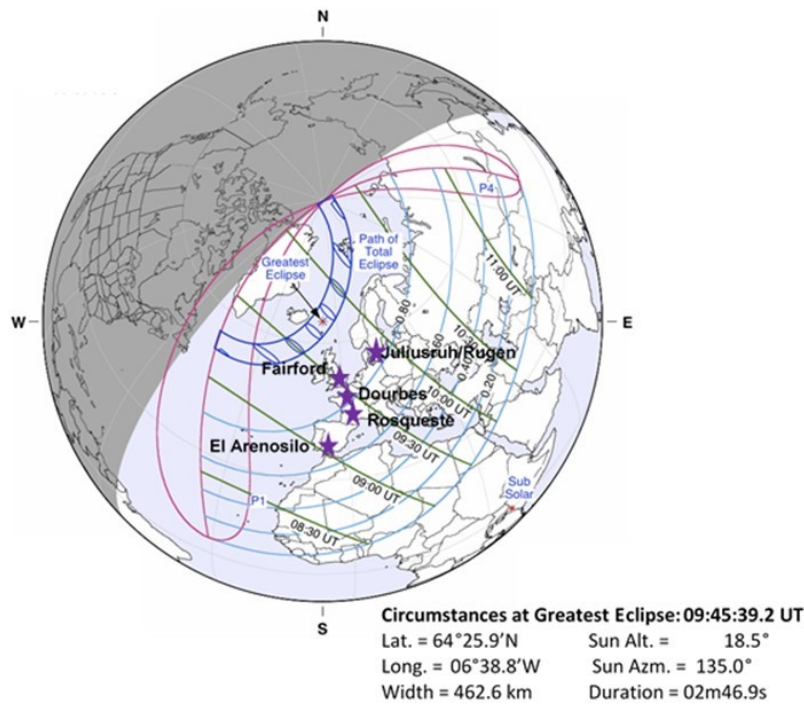


Figure 1. An orthographical map of the region covered, circumstances, and observation stations during the 20 March 2015 total solar eclipse. The faint blue lines indicate the area where the partial solar eclipse is seen and the thick blue lines is of the eclipse's maximum magnitude. The Circumstances at Greatest Eclipse: 09:45:39.2 UT, Latitude 64°25.9'N; Longitude 06°38.8'W; Width 462.6 km; Sun Altitude 18.5°; Sun Azimuth 135.0°; Duration is 02m46.9s. More details of its path can be seen via NASA (Total solar eclipse of 20 March 2015 <https://eclipse.gsfc.nasa.gov/>).

Table 1. The detailed information of Ionosonde stations, geographic coordinates, eclipse progression time frame, and maximum obscuration percentage during the March 20, 2015, total solar eclipse.

Station	Geographic Coordinate		Eclipse Start Time (UT)	Eclipse Max Time (UT)	Eclipse End Time (UT)	% of Max Obscuration	UT to LT difference (Approx.)
	Lat	Long	hh:mm:ss	hh:mm:ss	hh:mm:ss		
El Arenosilo	37.1	353.3	07:55:04.3	08:58:17.9	10:07:55.5	69.09	0
Roquestes	40.8	0.5	08:05:56.2	09:12:43.2	10:25:24.1	71.34	0
Dourbes	50.1	4.6	08:24:51.0	09:33:30.5	10:46:20.5	86.25	0
Fairford	51.7	358.5	08:22:45.9	09:29:29.2	10:40:34.4	94.17	0
Juliusruh	54.6	13.4	08:40:44.3	09:50:33.0	11:02:49.2	85.99	+1

10^{12} e/m^3 at 0915 LT, just a few minutes following the eclipse's maximum obscuration time. The removal of photoionisation of plasma caused by the passage of the moon's shadow over the atmosphere resulted in the delay period explained by the cooling, downwelling, and atmospheric expansion processes [31]. Also, it should be noted that the NmF2e varies with SIR. The ionisation constituents decrease as solar radiation decreases due to the moon's shadow on the ionosphere. The increase in NmF2e after the eclipse's maximum magnitude corresponds to an increase in O+, and thus an increase in ionisation through the eclipse's end time. The hmF2 recorded a distinct excursion; during the first contact of the eclipse, a gradual decrease in NmF2 was gradually uplifted to a higher altitude. The maximum peak height corresponded to the maximum decrease in NmF2, and the subsequent decrease in hmF2 explains the plasma species expansion process as a result of a gradual increase in electron density due to the increase in the photoionisation in the eclipse window's recuperation stage.

Over the ionosphere of Roquetes, Figure 2b, the minimum decrease in NmF2e was reached around 10 minutes following the eclipse's peak magnitude. This variation is contrary to the NmF2c variation, which increases throughout the eclipse window. The solar eclipse-caused valley recovered as the ionisation gained energy as the Moon gradually moved away from the alignment of the Sun's rays. This eclipse-induced plasma redistribution in the ionosphere is height dependent. The peak height corresponding to the maximum variation of electron density over Roquetes is presented in Figure 2bii. The hmF2e shows a special feature during the eclipse window, the hmF2e decrease at the beginning of the eclipse corresponded with the decrease in NmF2e. Following that, the hmF2e increases through the maximum eclipse magnitude period and reaches a peak value of 286 km at about 0925 LT. Thereafter, a sharp decrease was registered, with hmF2e reaching the minimum peak of ~229 km around 1025 LT, coinciding with the eclipse end time during the second phase of the window. This deviation of plasma

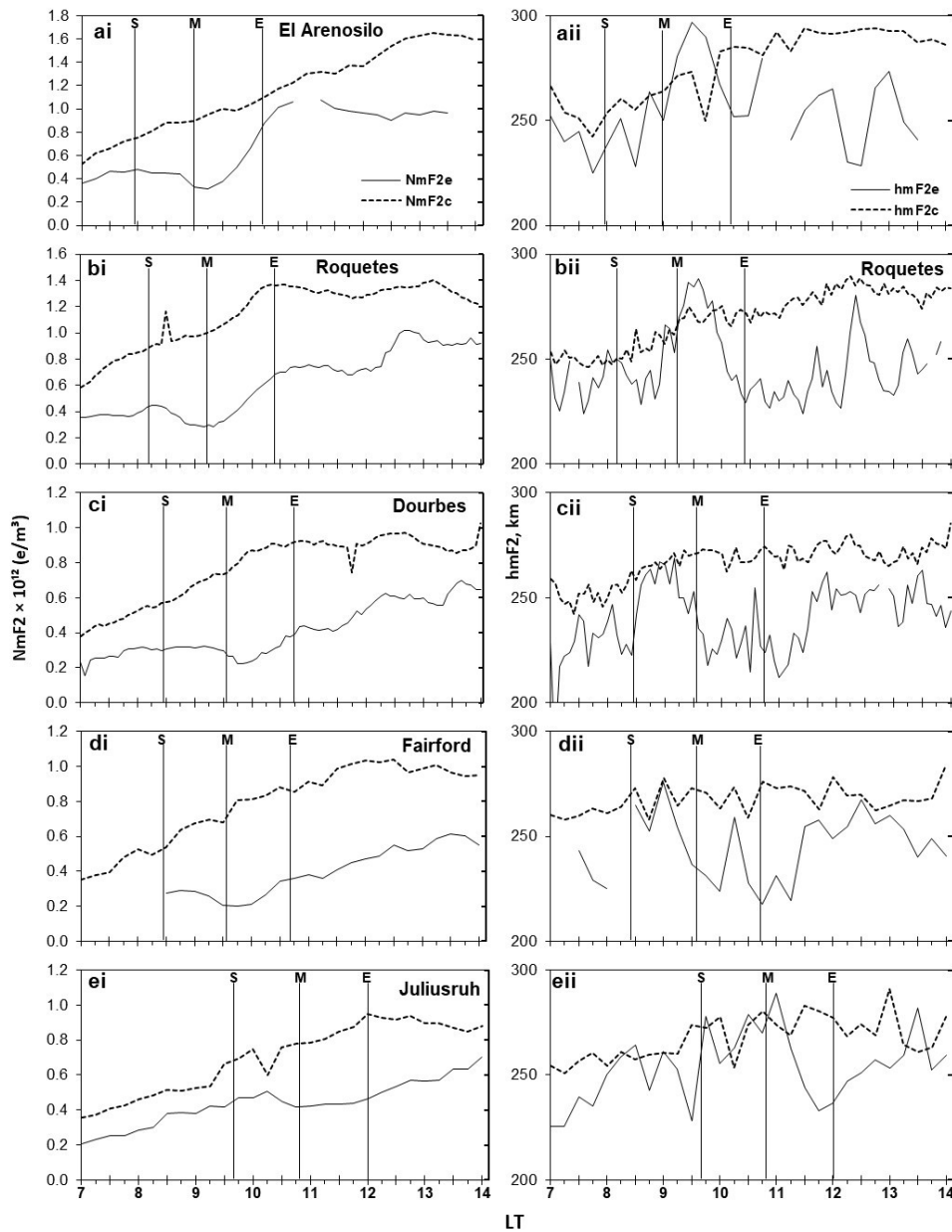


Figure 2. Variation of F2 region peak electron density, NmF2 and peak height, hmF2 during the solar eclipse. The vertical lines demonstrate the first contact or start time of the eclipse (s), the time of the maximum magnitude of the totality (M), and the last contact of the eclipse or the end time of the solar eclipse (E).

during the eclipse window as against that of the control day indicates that solar eclipse can cause plasma redistribution and, as a result, affect the transport process [4, 25].

The NmF2 and hmF2 variation in the ionosphere over Dourbes, Fairford and Juliusruh did not show any contrary behaviours and excursion compared to the El Arenosilo and Roquetes. The NmF2 depletion and its corresponding increase in hmF2 during the eclipse window is evidently due to the removal/reduction of photoionisation. Shortly after the eclipse's peak magnitude, the NmF2 decreased to its lowest point. This formation has been related to the diffusion processes; the downward diffusion/cooling process caused by the removal of the

SIR is associated with the increase in the nitrogen molecule, while the upward diffusion after total obscuration is due to the increase in the photoionisation [3, 4, 6, 13, 20, 31]. That is, solar eclipse can temporarily decrease the [O/N2] ratio due to the cooling of the thermosphere and the reduced efficiency of certain chemical reactions. The percentage deviation of the NmF2 at the eclipse window corresponds to the percentage obscuration of the solar eclipse, therefore as the percentage obscuration increases, so does the electron density deviation at the eclipse window. The percentage deviation over Fairford, Dourbes, and Juliusruh, with 94%, 86.25% and 85.99% obscuration is 74%, 73% and 50%, respectively. Adekoya *et al.* [2] observed that

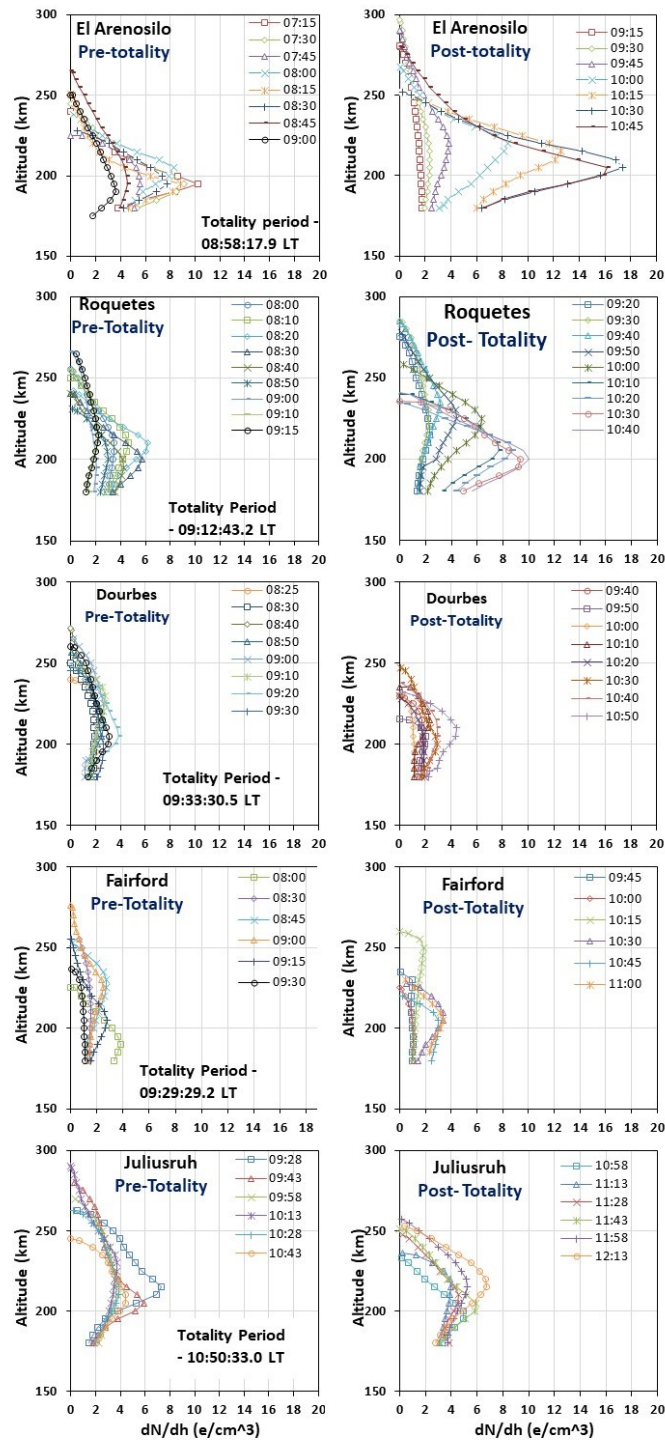


Figure 3. Electron ionisation gradient profile plots derived from the inversion of ionograms during the solar eclipse of 7 July 2019. All legends are in the local time (LT).

during the investigation of the solar eclipse of 21 August 2017, the plasma deviation decreased with decreasing percentage obscuration and used as a proxy in explaining the wind flow and thermospheric composition related to ionisation loss rate during the eclipse. Similarly, the increase in hmF2 following the eclipse's peak magnitude is conspicuous and concurrent, indi-

cating that plasma is indeed redistributed. The hmF2 plots show the varying values during the eclipse window compared to the control days. The increase in hmF2 during the eclipse is primarily caused by the reduction in solar extreme ultraviolet (EUV) radiation, which affects the ionisation and recombination processes in the F2 layer. From the point of view of NmF2 varia-

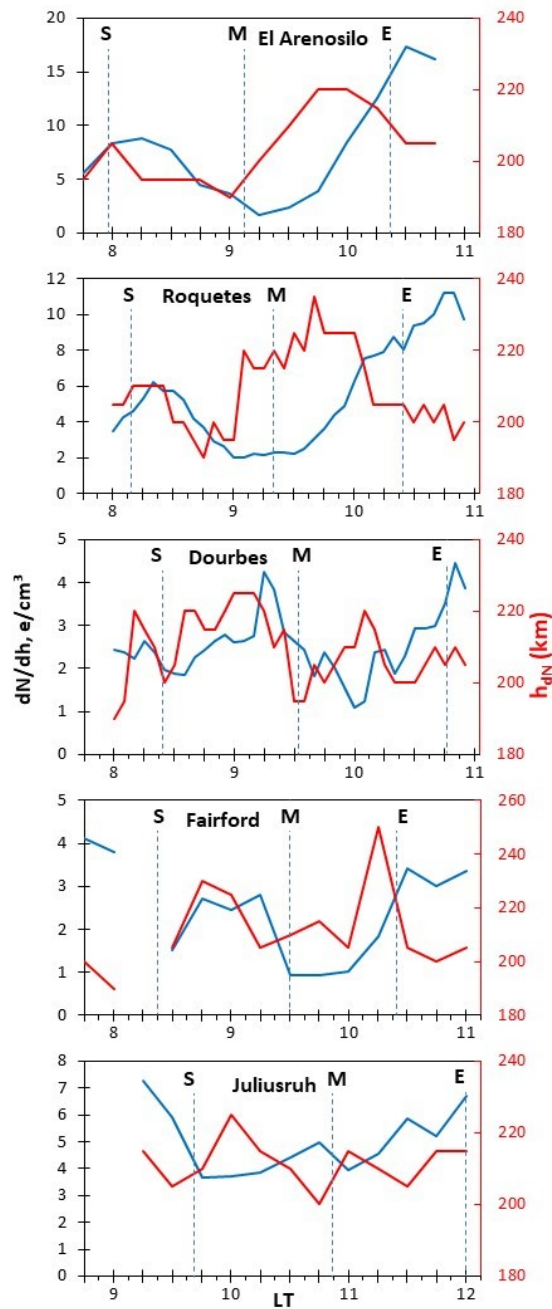


Figure 4. The pattern of ionisation gradient distribution during the solar eclipse progression (blue line) and the height corresponding to the respective positions of the maximum dN/dh magnitude, h_{dN} (red line).

tion, it shows that ionisation decreases during the eclipse window, which subsequently leads to changes in the plasma density and altitude. The vertical transport of plasma related to the hmF2 increase [2, 4] is influenced by the increase in the neutral winds in the ionosphere. The atmospheric dynamic wave motions cause changes in the neutral winds [30]. Therefore, the changes in photoionisation of chemical species and plasma dynamics caused changes in the reflection and modification of ionospheric F2 region formation during the solar eclipse window [6, 13, 44].

3.2. The Ionisation gradient (dN/dh) observation and pattern during the solar eclipse

Figure 3 depicts the typical ionisation gradient profile during the eclipse window, as presented for the stations within the obscuration of the solar eclipse. The first column shows the dN/dh at the first phase of the eclipse window (Pre-totally through the maximum magnitude of eclipse periods), and the second column shows the dN/dh at the second phase (post-totally periods). All of the gradient profiles revealed that the gradient distribution decreases with time during the pre-totally

period and reverses during the post-totally period. The increase in ionisation gradient during the post-totally period compared to the pre-totally period suggests the increasing ionisation due to the increasing solar radiation around the periods. The ionisation gradient was lower on average around the totality period than before and after. The minimum ionisation gradient appeared to be around the peak magnitude of the eclipse for all the stations, while the maximum appeared to be around the pre-totally and post-totally of the solar eclipse. It is important to note that while the ionisation gradient began at a height of 180 km altitude, which is the vertical height of the ionospheric F2-layer datum level, all of the gradient profiles occurred at an altitude above 200 km during the eclipse phases.

Figure 4 depicts a clear picture of the pattern of the ionisation gradient during the solar eclipse progression; the peak values of the ionisation gradient and their corresponding height (h_{dN}) magnitudes were quantitatively obtained for each station. From Figure 4, the ionisation gradient variation corresponds to the NmF2e variation. The peak response of dN/dh and its height (h_{dN}) at the second phase of the eclipse window informed that electron concentrations are spread over a large height range [45] where recombination is less significant. Also, it was observed that the time of the minimum ionisation gradient does not correspond with the time when the eclipse reaches its maximum magnitude. At each station, the minimum ionisation gradient was observed around 11 – 20 minutes after the totality period. In general, the ionisation gradient pattern appeared to follow the pattern of plasma diffusion and transport processes during the eclipse and related to the SIR. The delay time between the minimum ionisation gradient and the maximum magnitude of the solar eclipse has been related to the slower rate of charge transfer due to the gradual emergence of solar radiation [31] and recombined more rapidly compared to other periods at the eclipse window. Moreover, Adekoya and Chukwuma [31] revealed that the solar eclipse window is related to the sunset period, during which charges are gradually transferred to a region of a high recombination state.

3.3. The synergy between ionisation gradient and plasma distribution mechanisms at mid-latitude during a solar eclipse

In the mid-latitude ionospheric region, transport mechanisms, production, recombination, and diffusion processes influence plasma density distribution [4]. Understanding the plasma transport processes during an eclipse is important because variations in local solar ionising radiation affect the plasma ionisation at F2 region heights. According to Le *et al.* [44], transport processes/plasma movement are the main mechanisms in the F2 layer that drive the ionospheric plasma, which is connected to the background characteristics such as hmF2, local time, solar activity, and magnetic dip. During a solar eclipse, SIR is obscured totally or partially, changing the daily plasma distribution processes and causing significant changes in the F - region plasma density, resulting in a change in the daily F2 region morphology. At equatorial/low latitudes, the ionisation gradient represents a reversed electrodynamics drift of a plasma [35]. Herein, the plasma diffusion at mid-latitude

is synonymous with the ionisation gradient during the eclipse window, as it is the primary mechanism for plasma distribution. That is, downward and upward diffusion processes correspond to the decrease and increase in the ionisation gradient, respectively. During solar eclipse, solar radiation is partially lost and the molecular gases (N_2 and O_2) become the dominant chemical species [6, 20]. An increase in molecular nitrogen gas [N_2] dominates the first phase of the eclipse window, instigating the downward diffusion process during the atmospheric cooling process (the reduction in temperature resulting from the decrease in solar radiation) caused by the eclipse shadow. However, the second phase of the eclipse window is associated with the increase in atomic gas due to the gradual intensification in photoionisation after the totality period of the solar eclipse.

Chukwuma and Adekoya [4] extrapolated the vertical transport process at mid-latitude during a solar eclipse, taking into account the equilibrium state of the Chapman equation for the F2 layer, which is governed by the plasma's production, loss, diffusion and transport term. According to their findings, the plasma transport process varies with diffusion processes, decreasing during the first half of the eclipse phase and increasing after the maximum phase period. Similarly, the observed ionisation gradient follows a pattern similar to the diffusion and transport processes during the solar eclipse. During the eclipse's first phase, through the maximum magnitude, the dN/dh decreases. Around this period, the SIR decreases due to the shadow cast by the moon during its progression in the alignment between the Sun and the Earth. As shown in Figure 4, the ionisation element is reduced, increasing the molecular concentration of Nitrogen [O/N_2] and thus decreasing the ionisation gradient. Chukwuma and Adekoya [4] called this the cooling process, the process in which the N_2 increases due to the decrease in temperature and reduced solar radiation, hence the atmosphere's compression/contraction or upwelling [10]. Atmosphere contraction is the process in which the atomic chemical concentration in the atmosphere [O/N_2] decreases, typically due to cooling processes. Upwelling processes can occur due to various factors such as temperature differences, pressure gradients, or circulation patterns [23, 46–49]. In the context of nitrogen concentration during a solar eclipse, upwelling can play a role in redistributing nitrogen-rich air masses within the atmosphere to higher altitudes. That is, thermospheric composition [O/N_2] is lower when upwelling occurs in the upper atmosphere during a solar eclipse, while downwelling increases it. Upwelling processes can transport increased nitrogen molecules to higher altitudes (NmF2 and hmF2 observation depicted during the eclipse window) where recombination is less prominent. As depicted in Figure 2, one can see that the NmF2 decreases to the minimum while hmF2 reaches the peak height at the corresponding time during the solar eclipse phase. After the Sun's radiation to the Earth is completely obscured, the Moon gradually moves away from the Sun-Earth alignment, and the Earth's atmosphere begins to gain energy and plasma becomes ionized. The increase in plasma temperature leads to atmospheric expansion and downwelling, and thus an increase in ionisation thereafter. Martínez-Ledesma *et al.* [3] observed a significant cooling of electron and oxygen ion temperatures corresponding to a

large reduction of electron concentration. Müller-Wodarg *et al.* [6] and Le *et al.* [1] ascribed the changes observed during the eclipse window in the mid-latitude to changes in the diffusion mechanisms. Chukwuma and Adekoya [4] related this to modifications in the processes of plasma vertical transport, asserting that the processes of downward and upward diffusion were connected to the downward and upward vertical transport of plasma during the eclipse window. Therefore, the changes in the ionisation gradient, vertical transport and diffusion processes were explained by the behaviour of the F2-layer plasma during the short-term removal of solar ionising radiation. In a nutshell, the decrease in ionisation gradient is connected to the downward diffusion flux of plasma and this will cause a decrease in the electron density of the F2 region during the eclipse's first phase. Moreover, the increase is due to the upward diffusion.

On the right side of Figure 4, the height (h_{dN}) corresponding to the maximum ionisation gradient value for each period through the eclipse window is shown (red colour). When the h_{dN} is compared to the peak height (hmF2), it is discovered that they exhibit a similar structure and explain the plasma behaviour during the solar eclipse episode. The decrease in ionisation gradient during the second phase of the eclipse window corresponds to the increase in the h_{dN} . Also, it was observed that the maximum peak of h_{dN} was recorded not at the maximum magnitude of the eclipse, but rather during the period when the SIR was gradually restored. The h_{dN} peak response time does not coincide with that of the dN/dh . The hmF2 peak response at the eclipse window is higher than the h_{dN} across all the stations within the solar eclipse's path. The increase in hmF2 after the maximum magnitude of a solar eclipse is believed to be the result of photoionisation resurgence, which caused the upward vertical transport and uplifted plasma to the region of less recombinational processes [2, 4]. The ionisation gradient height exhibits the same characteristic as the h_{dN} increasing and reaching the maximum gradient peak after the totality period. Unlike the NmF2 and hmF2, whose peak response times often coincide, the peak response time and peak height of the ionisation gradient differ, but only during the second phase of the eclipse window. As observed from the stations, the h_{dN} delay time ranges between 25 and 40 mins, whereas the dN/dh delay time corresponds with NmF2. Therefore, it is then appropriate to suggest that the changes in ionisation gradient and its corresponding height are caused by the turnoff (obscuration) and onset effect of SIR on the background plasma distribution and vertical transport processes. Although plasma downward and upward vertical transports are related to plasma upwelling (downward diffusion/atmospheric compression) and downwelling (atmospheric expansion), they explain changes in thermospheric composition. The change in neutral composition, [O/N₂], accounted for the changes in the diffusion processes [6], resulting in variations in loss rates and ionisation production. Furthermore, the changes in the ionisation gradient during the eclipse window are connected to the degree of loss rate in ionisation (i.e., O⁺) caused by changes in neutral composition, which is controlled by variations in the local SIR. It should be noted that the emergence of the solar eclipse forced the chemical reaction to undergo rapid charge transfer processes

as it progressed. This was observed during the solar eclipse-induced ionisation process valley. Therefore, one can conclude that the pattern of the ionisation gradient is caused by the processes surrounding the solar eclipse and can affect the formation of the ionosphere, hence the radio wave signal disruption.

4. Conclusion

The pattern and variation of electron ionisation gradient as related to plasma distributions and transport processes at mid-latitudes were investigated during the total solar eclipse on March 20, 2015. The NmF2 varies with the SIR, with peak responses occurring 11 – 20 minutes after the eclipse's totality. The delay period is relative to the minimum reduction in NmF2 and the increase in hmF2 during the eclipse window's second phase. dN/dh recorded its minimum peak after the maximum magnitude of the eclipse as it decreased from the first contact of the eclipse through the totality period and increased after reaching the minimum peak during the second phase of the eclipse window. The solar eclipse-induced ionisation gradient valley was related to the vertical transport processes/diffusion processes. The height (h_{dN}) at which the maximum ionisation density was obtained showed a similar pattern with the hmF2. Unlike the hmF2, the time lag between the ionisation gradient's minimum peak and the eclipse's maximum magnitude ranges between 25 and 40 mins. Also, it was observed that the peak response of the h_{dN} is lower than that of the hmF2 across all stations. The changes in ionisation gradient and its corresponding height are due to the turnoff and onset effect of SIR on the background plasma distribution and vertical transport processes. Like diffusion and transport processes, the dN/dh explain the plasma changes in the ionosphere during the solar eclipse. The pattern of ionisation gradient can be caused by the ionospheric processes surrounding the solar eclipse and can affect the formation of the ionosphere, hence the radio wave signal disruption. Therefore, the dN/dh can be used to quantify the plasma anomaly at the ionospheric F2 layer.

Acknowledgement

We thank the World Data Centre for Geomagnetism, Kyoto (<http://wdc.kugi.kyoto-u.ac.jp/index.html>) for geomagnetic activity data, and ULMCAR (<https://giro.uml.edu/didbase/>) for providing global ionospheric Radio Observatory data. We greatly acknowledge the use of digital ionogram data from the Global Ionospheric Radio Observatory (GIRO) network, accessible via the online portal <https://giro.uml.edu/didbase/>. We express our gratitude to the service of the National Aeronautics and Space Administration, NASA Eclipse (<https://eclipse.gsfc.nasa.gov/SEdecade/SEdecade2011.html>) and National Space Science Data Centres (NSSDC's) OMNI database (<http://nssdc.gsfc.nasa.gov/omniweb>) for making available the information about the eclipse progression on the view of the Earth and the geomagnetic activity data. The use of the solar eclipse calculator from the Web address http://xjubier.free.fr/en/site_pages/SolarEclipseCalc_Diagram.html for progression and eclipse local-circumstance information is very helpful.

Data availability

The links to the ionogram dataset and the daily average data of the solar and planetary magnetic field indices used in this study are provided below, respectively:

- Ionogram dataset: <https://giro.uml.edu/didbase/>.
- Solar and planetary magnetic field indices: <https://omniweb.gsfc.nasa.gov/>.

References

- [1] H. Le, L. Liu, X. Yue, W. Wan & B. Ning, "Latitudinal dependence of the ionospheric response to solar eclipse", *Journal of Geophysical Research: Space Physics* **114** (2009) A07308. <http://dx.doi.org/10.1029/2009JA014072>.
- [2] B. J. Adekoya, B. O. Adebesein, T. W. David, S. O. Ikubanni, S. J. Adebisi, O. S. Bolaji & V. U. Chukwuma "Solar-eclipse-induced perturbations at mid-latitude during the 21 August 2017 event", *Annales Geophysicae* **37** (2019) 171. <https://doi.org/10.5194/angeo-37-171-2019>.
- [3] M. Martínez-Ledesma, M. Bravo, B. Urra, J. Souza & A. Foppiano "Prediction of the ionospheric response to the 14 December 2020 total solar eclipse using SUPIM-INPE", *Journal of Geophysical Research: Space Physics* **125** (2020) e2020JA028625. <https://doi.org/10.1029/2020JA028625>.
- [4] V. U. Chukwuma & B. J. Adekoya "The effects of March 20 2015 solar eclipse on the F2 layer in the mid-latitude", *Advances in Space Research* **58** (2016) 1720. <https://doi.org/10.1016/j.asr.2016.06.038>.
- [5] K. Cheng, Y. -N. Huang & S. -W. Chen, "Ionospheric effects of the solar eclipse of September 23, 1987, around the equatorial anomaly crest region". *Journal of Geophysical Research: Space Physics* **97** (1992) 103. <https://doi.org/10.1029/91JA02409>.
- [6] I. C. F. Müller-Wodarg, A. D. Aylward & M. Lockwood, "Effects of a Mid-Latitude Solar Eclipse on the Thermosphere and Ionosphere – A Modelling Study", *Geophysical Research Letter* **25** (1998) 3787. <https://doi.org/10.1029/1998GL900045>.
- [7] C. J. Davis, M. Lockwood, S. A. Bell, J. A. Smith & E. M. Clarke, "Ionospheric measurements of relative coronal brightness during the total solar eclipses of 11 August, 1999 and 9 July, 1945", *Annales Geophysicae* **18** (2000) 182. <https://doi.org/10.1007/s00585-000-0182-z>.
- [8] C. J. Davis, E. M. Clarke, R. A. Bamford, M. Lockwood & S. A. Bell, "Long term changes in EUV and X-ray emissions from the solar corona and chromosphere as measured by the response of the Earth's ionosphere during total solar eclipses from 1932 to 1999", *Annales Geophysicae* **19** (2001) 263. <https://doi.org/10.5194/angeo-19-263-2001>.
- [9] E. L. Afraimovich, E. A. Kosogorov & O. S. Lesyuta, "Effects of the August 11, 1999 total solar eclipse as deduced from total electron content measurements at the GPS network", *Journal of Atmospheric and Solar-Terrestrial Physics* **64** (2002) 1933. [https://doi.org/10.1016/S1364-6826\(02\)00221-3](https://doi.org/10.1016/S1364-6826(02)00221-3).
- [10] P. Sauli, P. Abry, J. Boska & L. Duchayne, "Wavelet characterization of ionospheric acoustic and gravity waves occurring during the solar eclipse of 11 August 1999", *Journal of Atmospheric and Solar-Terrestrial Physics* **68** (2006) 586. <https://doi.org/10.1016/j.jastp.2005.03.024>.
- [11] J. J. Curto, B. Heilig & M. Piñol, "Modeling the geomagnetic effects caused by the solar eclipse of 11 August 1999", *Journal of Geophysical Research: Space Physics* **111** (2006) A07312. <http://dx.doi.org/10.1029/2005JA011499>.
- [12] N. Jakowski, S. M. Stankov, V. Wilken, C. Borries, D. Altadill, J. Chum, D. Buresova, J. Boska, P. Sauli, F. Hruska & Lj. R. Cander, "Ionospheric behaviour over Europe during the solar eclipse of 3 October 2005". *Journal of Atmospheric and Solar-Terrestrial Physics* **70** (2008) 836. <https://doi.org/10.1016/j.jastp.2007.02.016>.
- [13] E. I. Grigorenko, M. V. Lyashenko & L. F. Chernogor, "Effects of the Solar Eclipse of March 29, 2006, in the Ionosphere and Atmosphere", *Geomagnetism and Aeronomy* **48** (2008) 337. <https://doi.org/10.1134/S0016793208030092>.
- [14] H. Le, L. Liu, F. Ding, Z. Ren, Y. Chen, W. Wan, B. Ning, X. Guirong, M. Wang, G. Li, B. Xiong & H. Lianhuan, "Observations and modeling of the ionospheric behaviors over the east Asia zone during the 22 July 2009 solar eclipse", *Journal of Geophysical Research: Space Physics* **115** (2010) A10313. <https://doi.org/10.1029/2010JA015609>.
- [15] X. Wang, J. J. Berthelier & J. P. Lebreton, "Ionosphere variations at 700 km altitude observed by the DEMETER satellite during the 29 March 2006 solar eclipse", *Journal of Geophysical Research: Space Physics* **115** (2010) A11312. <https://doi.org/10.1029/2010JA015497>.
- [16] A. Paul, T. Das, S. Ray, A. Das, D. Bhowmick & A. DasGupta, "Response of the equatorial ionosphere to the total solar eclipse of 22 July 2009 and annular eclipse of 15 January 2010 as observed from a network of stations situated in the Indian longitude sector", *Annales Geophysicae* **29** (2011) 1955. <https://doi.org/10.5194/angeo-29-1955-2011>.
- [17] M. V. Lyashenko & L. F. Chernogor, "Solar eclipse of August 1, 2008, over Kharkov: 3. calculation results and discussion", *Geomagnetism and Aeronomy* **53** (2013) 367. <http://dx.doi.org/10.1134/S0016793213020096>.
- [18] Y. J. Chuo, "Ionospheric effects on the F region during the sunrise for the annular solar eclipse over Taiwan on 21 May 2012", *Annales Geophysicae* **31** (2013) 1891. <https://doi.org/10.5194/angeo-31-1891-2013>.
- [19] N. Scafetta & A. Mazzarella, "Effects of March 20, 2015, partial (~50%) solar eclipse on meteorological parameters in the urban area of Naples (Italy)", *Annals of Geophysics* **59** (2016) A0106. <https://doi.org/10.4401/ag-6899>.
- [20] H. Rishbeth, "Solar eclipses and ionospheric theory", *Space Science Review* **8** (1968) 543. <https://doi.org/10.1007/BF00175006>.
- [21] B. J. Adekoya & V. U. Chukwuma, "Response of the mid-latitude ionospheric F2 to total solar eclipses of solar cycle 23", *Indian Journal of Radio Science and Space Physics* **41** (2012) 594. <https://nopr.nisr.res.in/handle/123456789/15634>.
- [22] B. G. Fejer, "The electrodynamics of the low-latitude ionosphere: recent results and future Challenges", *Journal of Atmospheric and Solar-Terrestrial Physics* **59** (1997) 1465. [https://doi.org/10.1016/S1364-6826\(96\)00149-6](https://doi.org/10.1016/S1364-6826(96)00149-6).
- [23] B. O. Adebesein, B. J. Adekoya & T. W. David, "Plasma transport process in the equatorial/low-latitude ionosphere", *Advances in Space Research* **63** (2019) 1619. <https://doi.org/10.1016/j.asr.2018.11.013>.
- [24] B. O. Adebesein, J. O. Adeniyi, I. A. Adimula & B. W. Reinisch, "Equatorial vertical plasma drift velocities and electron densities inferred from ground-based ionosonde measurements during low solar activity", *Journal of Atmospheric and Solar-Terrestrial Physics* **97** (2013) 58. <https://doi.org/10.1016/j.jastp.2013.02.010>.
- [25] B. J. Adekoya, V. U. Chukwuma & B. W. Reinisch, Ionospheric vertical plasma drift and electron density response during total solar eclipses at equatorial/low latitudes. *Journal of Geophysical Research: Space Physics* **120** (2015) 8066. <https://doi.org/10.1002/2015JA021557>.
- [26] A. Meza, G. Bosch, M. P. Natali & B. Eylonstein "Ionospheric and geomagnetic response to the total solar eclipse on 21 August 2017", *Advances in Space Research* **69** (2022) 16. <https://doi.org/10.1016/j.asr.2021.07.029>.
- [27] C. O. Hines, "Internal atmospheric gravity waves at ionospheric heights", *Canadian Journal of Physics* **38** (1960) 1441. <https://doi.org/10.1139/p60-150>.
- [28] G. L. Goodwin & G. J. Hobson, "Atmospheric gravity waves generated during a solar eclipse", *Nature* **275** (1978) 109. <https://doi.org/10.1038/275109a0>.
- [29] B. W. Jones, "A search for atmospheric pressure waves from the total solar eclipse of 9 March 1997", *Journal of Atmospheric and Solar-Terrestrial Physics* **61** (1999) 1017. [https://doi.org/10.1016/S1364-6826\(99\)00073-5](https://doi.org/10.1016/S1364-6826(99)00073-5).
- [30] H. Rishbeth, K. J. F. Sedgemore-Schlthess & T. Ulich, "Semiannual and annual variations in the height of the ionospheric F2-peak" *Annales Geophysicae* **18** (2000) 285. <https://doi.org/10.1007/s00585-000-0285-6>.
- [31] B. J. Adekoya & V. U. Chukwuma, "Ionospheric F2 layer responses to total solar eclipses at low- and midlatitude", *Journal of Atmospheric and Solar-Terrestrial Physics* **138** (2016) 136. <https://doi.org/10.1016/j.jastp.2016.01.006>.
- [32] W. Wang, T. Dang, J. Lei, S. Zhang, B. Zhang & A. Burns, "Physical processes driving the response of the F2 region ionosphere to the 21 August 2017 solar eclipse at Millstone Hill", *Journal of Geophysical Research:*

- Space Physics **124** (2019) 2978. <https://doi.org/10.1029/2018JA025479>.
- [33] M. Yasar, "The change of diffusion processes for $O^{++} N_2 \rightarrow NO^{++} N$ reaction in the ionospheric F region during the solar eclipse over Kharkov", Thermal Science **25** (2021) 51. <https://doi.org/10.2298/TSCI200521006Y>.
- [34] R. Atici & S. Sağır, "The Variation of Ionospheric TEC During Solar Eclipse on March 20, 2015". Celal Bayar University Journal of Science **18** (2022) 403. <https://dergipark.org.tr/en/pub/cbayarfbe/issue/74009/1019000>.
- [35] B. O. Adebesein, J. O. Adeniyi, O. A. Oladipo, A. O. Olawepo & I. A. Adimula, "Quantitative Characteristics of Equatorial Ionisation Gradient above 150 km at Low Solar Activity", Radio Science **53** (2018) 948. <https://doi.org/10.1029/2018RS006560>.
- [36] B. W. Reinisch & I. A. Galkin, "Global Ionosphere Radio Observatory (GIRO)", Earth Planets Space **63** (2011) 377. <https://doi.org/10.5047/eps.2011.03.001>.
- [37] B. W. Reinisch, & X. Huang, "Automatic calculation of electron density profiles from digital ionograms 3. Processing of bottomside ionograms", Radio Science **18** (1983) 477. <https://doi.org/10.1029/RS018i003p00477>.
- [38] I. A. Galkin, G. M. Khmyrov, B. W. Reinisch & J. McElroy, "The SAOXML 5: New Format for Ionogram-Derived Data", AIP Conference Proceedings **974** (2008) 160. <https://doi.org/10.1063/1.2885025>.
- [39] X. Huang & B. W. Reinisch, "Vertical electron density profiles from the digisonde network", Advances in Space Research **18** (1996) 121. [https://doi.org/10.1016/0273-1177\(95\)00912-4](https://doi.org/10.1016/0273-1177(95)00912-4).
- [40] R. Ma, J. Xu, W. Wang & W. Yuan, "Seasonal and latitudinal differences of the saturation effect between ionospheric NmF2 and solar activity indices", Journal of Geophysical Research: Space Physics **114** (2009) A10303. <https://doi.org/10.1029/2009JA014353>.
- [41] B. J. Adekoya & B. O. Adebesein, "Hemispheric, seasonal and latitudinal dependence of storm-time ionosphere during low solar activity period", Advances in Space Research **54** (2014) 2184. <https://doi.org/10.1016/j.asr.2014.08.013>.
- [42] B. O. Adebesein, J. O. Adeniyi, I. A. Adimula, S. J. Adebisi, S. O. Ikubanni, O. A. Oladipo & A. O. Olawepo, "Pattern of ionisation gradient, solar quiet magnetic element, and F2-layer bottomside thickness parameter at African equatorial location", Radio Science **54** (2019) 415. <https://doi.org/10.1029/2018RS006742>.
- [43] B. O. Adebesein, J. O. Adeniyi, I. A. Adimula, S. J. Adebisi, S. O. Ikubanni & B. J. Adekoya, "Current understanding of the equatorial E B drift velocities in the African sector: a short review" Journal of the Nigerian Society of Physical Science **4** (2022) 54. <https://journal.nspss.org.ng/index.php/jnspss/article/view/327>.
- [44] H. Le, L. Liu, X. Yue & W. Wan, "The Mid-latitude F2 layer during solar eclipses: observations and modelling", Journal of Geophysical Research **113** (2008) A08309. <http://dx.doi.org/10.1029/2007JA013012>.
- [45] S. M. Radicella & J. O. Adeniyi, "Equatorial ionospheric electron density below the F2 peak", Radio Science **34** (1999) 1153. <https://doi.org/10.1029/1999RS900071>.
- [46] G. W. Pröss, "Ionospheric F region storms", in *Handbook of Atmospheric Electrodynamics*, CRC Press, 1995, pp. 195–248. <https://www.taylorfrancis.com/chapters/edit/10.1201/9780203713297-8/ionospheric-region-storms-gerd-pr%C3%B6ss>.
- [47] H. Rishbeth, "How the thermospheric circulation affects the ionospheric F2-layer", Journal of Atmospheric and Solar-Terrestrial Physics **60** (1998) 1385. [https://doi.org/10.1016/S1364-6826\(98\)00062-5](https://doi.org/10.1016/S1364-6826(98)00062-5).
- [48] M. J. Buonsantos, "Ionospheric Storms – A review", Space Science Reviews **88** (1999) 563. <https://doi.org/10.1023/A:1005107532631>.
- [49] J. S. Shim, M. Kuznetsova, L. Rastatter, M. Hesse, D. Bilitza, M. Butala, M. Codrescu, B. Emery, B. Foster, T. Fuller-Rowell, J. Huba, A. J. Mannucci, X. Pi, A. Ridley, L. Scherliess, R. W. Schunk, P. Stephens, D. C. Thompson, L. Zhu, D. Anderson, J. L. Chau, J. J. Sojka & B. Rideout, "CEDAR Electrodynamics Thermosphere Ionosphere (ETI) Challenge for systematic assessment of ionosphere/thermosphere models: NmF2, hmF2, and vertical drift using ground-based observations", Space Weather **9** (2011) S12003. <https://doi.org/10.1029/2011SW000727>.